886 *Chem. Mater.* **2011,** *23,* 886–895
DOI:10.1021/cm102329v

CHEMISTRY OF MATERIALS
Article

Structural Evolution of Evaporated Lead Phthalocyanine Thin Films for Near-Infrared Sensitive Solar Cells†

Karolien Vasseur,*[,‡,§] Barry P. Rand,[‡] David Cheyns,[‡] Ludo Froyen,[§] and Paul Heremans[‡,⊥]

[‡]*imec, Kapeldreef 75, B-3001 Leuven, Belgium,* [§]*Department of Metallurgy and Materials Engineering, Katholieke Universiteit Leuven, Kasteelpark Arenberg 44, B-3001 Leuven, Belgium, and* [⊥]*Department of Electrical Engineering, Katholieke Universiteit Leuven, Kasteelpark Arenberg 10, B-3001 Leuven, Belgium*

Received August 13, 2010. Revised Manuscript Received October 31, 2010

In this work, we focus on the deposition conditions as a means to control the structural evolution of lead phthalocyanine (PbPc) films in order to promote the triclinic structure, thereby inducing a shift in the absorption spectrum toward the near-infrared (NIR). Absorption spectra of PbPc films exhibit an enhanced NIR absorption peak at a wavelength of $\lambda = 900$ nm upon (i) increasing film thickness, (ii) increasing substrate temperature, or (iii) decreasing evaporation rate. X-ray diffraction measurements correlate the enhancement of the NIR absorption peak with an improved crystallinity and increased average volume of triclinic domains in the mixed monoclinic−triclinic films. As the surface structure of 10 and 60 nm thick films differ, this implies an asymmetric layer structure with a semicrystalline monoclinic film close to the substrate, evolving to a predominantly triclinic structure in the upper part of the film. We have demonstrated the use of structural control of the PbPc layer in a planar heterojunction solar cell with NIR-sensitivity. Decreasing the evaporation rate results in solar cells with significantly enhanced short-circuit current density (J_{SC}), because of the change in absorption in combination with the longer exciton diffusion length that was estimated for donor layers exhibiting a predominantly triclinic structure. Overall, an optimized solar cell yields a power conversion efficiency of 2.6% (2.1% when correcting for the solar spectrum mismatch), and has external quantum efficiencies above 11% from $\lambda = 320-990$ nm with a peak value of 34% at $\lambda = 900$ nm.

1. Introduction

Photovoltaic technology is being recognized as an essential component to meet future global energy needs. The potential of solar cells based on π-conjugated polymers or small molecules lies primarily in their compatibility with low-cost processing on large-area substrates.[1] Although a considerable improvement in power conversion efficiency (PCE) of organic solar cells has been made since the development of the donor/acceptor heterojunction concept by Tang,[2] this value needs to increase in order to render this technology commercially viable. One of the factors limiting the PCE is the narrow absorption window typical of organic semiconductors, which limits the overlap with the solar spectrum.[3] The tandem cell device architecture, consisting of stacked single heterojunction subcells that operate in different regions of the solar spectrum, is one approach for utilizing narrow-absorbing materials to ensure a broad spectral coverage.[4] As 50% of the total solar photon flux is at wavelengths between $\lambda = 600$ and 1000 nm, there is still a need for donor materials whose absorption extends to the near-infrared (NIR) while maintaining an efficient photon-to-current conversion.[5−9]

Among small-molecular weight semiconductors, phthalocyanines (Pc) are the most frequently used donor materials because of their excellent chemical stability, high absorption coefficients, and flexibility for chemical modification. Incorporation of different metal atoms into the Pc ring can significantly alter film morphology and packing structures, thereby offering the possibility to change the thin-film optical and electrical characteristics.[10] Planar Pcs, including metal-free Pc and many of the Pcs incorporating divalent central metals, such as Cu, Zn, Ni, Fe, and Co, crystallize in herringbone-like vertical stacks assigned to the α- or β-phases, which differ mainly by the tilting angle of the molecular plane with respect

† Accepted as part of the "Special Issue on π-Functional Materials".

*Corresponding author. E-mail: karolien.vasseur@imec.be. Phone: +32 16287876. Fax: +32 16 281097.

(1) Rand, B. P.; Genoe, J.; Heremans, P.; Poortmans, J. *Progr. Photovoltaics* **2007**, *15*, 659–676.
(2) Tang, C. W. *Appl. Phys. Lett.* **1986**, *48*, 183–185.
(3) Heremans, P.; Cheyns, D.; Rand, B. P. *Acc. Chem. Res.* **2009**, *42*, 1740–1747.
(4) Cheyns, D.; Rand, B. P.; Heremans, P. *Appl. Phys. Lett.* **2010**, *97*, 033301.
(5) Perez, M. D.; Borek, C.; Djurovich, P. I.; Mayo, E. I.; Lunt, R. R.; Forrest, S. R.; Thompson, M. E. *Adv. Mater.* **2009**, *21*, 1517–1520.
(6) Rand, B. P.; Xue, J.; Yang, F.; Forrest, S. R. *Appl. Phys. Lett.* **2005**, *87*, 233508.
(7) Li, N.; Lassiter, B. E.; Lunt, R. R.; Wei, G.; Forrest, S. R. *Appl. Phys. Lett.* **2009**, *94*, 023307.
(8) Bailey-Salzman, R. F.; Rand, B. P.; Forrest, S. R. *Appl. Phys. Lett.* **2007**, *91*, 013508.
(9) Chauhan, K. V.; Sullivan, P.; Yang, J. L.; Jones, T. S. *J. Phys. Chem. C* **2010**, *114*, 3304–3308.
(10) Claessens, C. G.; Hahn, U.; Torres, T. *Chem. Rec.* **2008**, *8*, 75–97.

 Published on Web 11/17/2010

to the stacking axis.[11,12] Because of the very similar packing, films with different polymorphs exhibit a similar absorption spectrum with the most intense Q-band peak typically between $\lambda = 500$ and 750 nm.[13] Nonplanar phthalocyanines are also known to be polymorphic, but packing arrangements can differ considerably due to the decreased symmetry of these pyramidal-shaped molecules. In particular, intermolecular interactions vary with different packing structures,[14,15] causing optical and electrical characteristics of these compounds to change considerably upon phase transition.

For lead phthalocyanine (PbPc), as for the other nonplanar Pcs, the two predominant polymorphs have the monoclinic and triclinic crystal structure. In the monoclinic crystal, the PbPc molecules are stacked in linear columns parallel to the *c*-axis, leading to behavior characteristic of a one-dimensional conductor.[16] In the triclinic crystal structure, the molecules stack along the *a*-axis orienting their convex and concave sides alternately.[17] As was observed for TiOPc and VOPc, this stacking arrangement induces an increased $\pi-\pi$ interaction between adjacent Pc rings, causing broadening of the Q-band spectrum toward the NIR.[13,18−20] The influence of the molecular orientation on the band-edge energies of TiOPc and PbPc are thoroughly discussed in ref 21.

The vastly different optoelectronic characteristics of the monoclinic and triclinic PbPc polymorph make controlling the PbPc film structure crucial for optimizing device operation. Phase transitions have been achieved by templating using different substrates[22] and substrate treatments,[23] postdeposition annealing,[24,25] applying pressure,[26] or changing deposition conditions.[27,28] The obtained control over PbPc film structure has been applied for optimization of switches, thin film transistors[29] and gas sensors,[24,27] but was never exploited for solar cell applications. The use of PbPc as a donor material in organic solar cells deposited on top of a ZnPc templating layer has been reported, giving an optimized PCE of 1.95%.[30] However, information on the achieved PbPc phase and its concomitant influence on solar cell performance is lacking.

Interestingly, the short-circuit current density (J_{SC}) of single heterojunction solar cells based on TiOPc was doubled upon TiOPc phase transition from monoclinic to triclinic.[13] As the most intense absorption peak of the NIR absorbing phase of TiOPc is situated at shorter wavelengths than that of the triclinic PbPc polymorph, which exhibits a maximal absorption at $\lambda = 900$ nm,[24] the gain in J_{SC} for solar cells based on the triclinic PbPc phase could be even higher, rendering this material a very promising candidate to achieve high-performance NIR-sensitive solar cells.

In this work, we aim to gain insight as to the correlation between solar cell parameters and the structure of the PbPc donor layer they are based on, in order to validate the possibilities of this material for the fabrication of NIR-sensitive solar cells. First, variations of substrate temperature and deposition rate are correlated with structural evolution of the film as assessed by both absorption spectroscopy and X-ray diffraction measurements, whereas film topography is investigated with atomic force microscopy (AFM). We then study the consequences of the donor layer structure and its crystallinity on the spectral response in planar heterojunction solar cells.

2. Experimental Methods

The substrates used in this study are glass substrates with 80 nm thick prepatterned indium−tin-oxide (ITO, Kintec) and highly doped n^{+2}-type silicon wafers with thermally grown SiO_2. Substrate cleaning consisted of sonication in detergent, deionized water and acetone, followed by submersion in hot isopropanol. Finally, a 15 min ultraviolet-O_3 treatment was applied prior to deposition.

The organic materials, PbPc ($C_{32}H_{16}N_8Pb$, Sigma-Aldrich), fullerene (C_{60}, SES research) and bathocuproine or BCP ($C_{26}H_{20}N_2$, Sigma-Aldrich) were purified at least once using gradient sublimation, while Ag was used as received. Thin films of PbPc were deposited by thermal evaporation in a high vacuum evaporator with a base pressure below 5×10^{-7} Torr. The temperature of the PbPc evaporation cell varied between 300 and 340 °C, and between 325 and 350 °C in order to achieve a stable deposition rate (r_{dep}) of 0.2 Å/s and 1 Å/s, respectively, as monitored by a quartz crystal microbalance. Substrate temperatures (T_{sub}) of 35 °C, without heating, and 70 °C have been used. For solar cell structures, subsequent layers were deposited in the same system without breaking the vacuum. No substrate heating was applied during deposition of these layers. The Ag cathode is evaporated through a shadow mask, defining an active area of 0.134 cm^2.

Absorption spectra of the films on glass were measured between 300 and 1100 nm with a Shimadzu UV-1601PC UV−visible spectrophotometer. Optical constants are measured using spectroscopic ellipsometry (SOPRA, ges5). Topography of the

(11) Heutz, S.; Bayliss, S. M.; Middleton, R. L.; Rumbles, G.; Jones, T. S. *J. Phys. Chem. B* **2000**, *104*, 7124–7129.
(12) Gould, R. D. *Coord. Chem. Rev.* **1996**, *156*, 237–274.
(13) Placencia, D.; Wang, W.; Shallcross, R. C.; Nebesny, K. W.; Brumbach, M.; Armstrong, N. R. *Adv. Funct. Mater.* **2009**, *19*, 1913–1921.
(14) Yanagi, H.; Imamura, M.; Ashida, M. *J. Appl. Phys.* **1994**, *75*, 2061–2068.
(15) Gastonguay, L; Veilleux, G.; Cote, R.; Saint-Jacques, R. G.; Dodelet, J. P. *Chem. Mater.* **1993**, *5*, 381–390.
(16) Ukei, K. *Acta Crystallogr., Sect. B* **1973**, *29*, 2290–2292.
(17) Iyechika, Y.; Yakushi, K.; Ikemoto, I.; Kuroda, H. *Acta Crystallogr., Sect. B* **1982**, *38*, 766–770.
(18) Hosoda, M.; Wada, T.; Yamada, A.; Garito, A. F.; Sasabe, H. *Jpn. J. Appl. Phys.* **1991**, *30*, L 1486–L 1488.
(19) Janczak, J.; Idemori, Y. M. *Polyhedron* **2003**, *22*, 1167–1181.
(20) Orti, E.; Bredas, J. L.; Clarisse, C. *J. Chem. Phys.* **1990**, *92*, 1228–1235.
(21) Yamane, H.; Honda, H.; Fukagawa, H.; Ohyama, M.; Hinuma, Y.; Kera, S.; Okudaira, K. K.; Uneo, N. *J. Electron. Spectrosc. Relat. Phenom.* **2004**, *137−140*, 223–227.
(22) Mizoguchi, K.; Mizui, K.; Kim, D.; Nakayama, M. *Jpn. J. Appl. Phys.* **2002**, *41*, 6421–6425.
(23) Tabuchi, S.; Tabata, H.; Kawi, T. *Surf. Sci.* **2004**, *571*, 117–127.
(24) Campbell, D; Collins, R. A. *Thin Solid Films* **1995**, *261*, 311–316.
(25) Ottaviano, L.; Lozzi, L.; Phani, A. R.; Ciattoni, A.; Santucci, S.; Di Nardo, S. *Appl. Surf. Sci.* **1998**, *136*, 81–86.
(26) Sakata, M.; Sumimoto, M.; Gushima, M.; Fujimoto, H.; Matsuzaki, S. *Solid State Commun.* **2002**, *121*, 363–366.
(27) Collins, R. A.; Krier, A.; Abass, A. K. *Thin Solid Films* **1993**, *229*, 113–118.
(28) Miyamoto, A.; Nichogi, K.; Taomoto, A.; Nambu, T.; Murakami, M. *Thin Solid Films* **1995**, *256*, 64–67.
(29) Tabuchi, S.; Otsuka, Y.; Kanai, M.; Tabata, H.; Matsumoto, T.; Kawai, T. *Org. Electr.* **2010**, *11*, 916–924 and references herein.
(30) Dai, J.; Jiang, X.; Wang, H.; Yan, D. *Appl. Phys. Lett.* **2007**, *91*, 253503.

Table 1. Calculated Peak Positions and Corresponding Reflection Planes for the Monoclinic (M) and Triclinic (T) Phases Used in the XRD Analysis

peak position (deg)	phase	reflection plane
6.93	M	(2 0 0)
6.95	T	(0 0 1)
7.37	T	(1 $\bar{1}$ 0)
7.47	T	(1 0 0)
7.75	M	(1 2 0)
12.12	T	(0 2 0)
12.35	T	(1 1 $\bar{1}$)
12.52	M	(3 $\bar{2}$ 0)
13	T	(1 $\bar{2}$ 1)
16.49	T	(1 1 $\bar{2}$)
16.52	T	(1 $\bar{3}$ 0)
16.64	T	(2 $\bar{2}$ 1)

films on ITO was assessed by AFM, using a Picoscan PicoSPM LE scanning probe in tapping mode. X-ray diffraction measurements were performed on a PANalytical X′Pert Pro Materials Research Diffractometer using Cu Kα radiation. The XRD measurements were performed on 10 and 60 nm thick PbPc films deposited on SiO_2 substrates. To minimize the substrate contribution to the XRD profile, we used an incident angle of 0.2° such that only the top surface of the film is probed.[31] An integration time of 10 s per 0.005° was used for scanning 2θ.

The analysis of the XRD patterns requires a deconvolution of the measured peaks, as diffraction peaks from the monoclinic (M) and triclinic (T) crystal structures are situated very close to each other, or even coincide. Therefore, diffraction patterns for both crystal structures have been simulated based on the respective unit-cell parameters[16,17] with the program CaRIne (v3.1). The resolved peaks from the measured XRD pattern are then fitted to the simulated XRD pattern by taking into account only those peaks with an intensity larger than 20% of the most intense peak. Positions of the calculated diffraction peaks used for deconvolution and their assigned reflection planes are listed in Table 1.

Current density−voltage characteristics of photovoltaic cells were measured in dark and under simulated solar light, using a Keithley 2602 in combination with an Abet solar simulator, calibrated to produce 100 mW/cm^2 AM1.5G illumination. In the EQE setup, light from Xe and quartz halogen lamps were coupled into a monochromator and their intensities calibrated with a Si photodiode. The light incident on the device was chopped and the modulated current signal detected with current−voltage and lock-in amplifiers.

The spectral response data is fitted by transfer matrix modeling[32] in order to extract exciton diffusion lengths. First, the measured optical constants for different film thicknesses are used to model the PbPc films as a superposition of uniform 20 nm thick layers. The first layer of 20 nm thickness is successfully fit with a single layer. Then, the optical constants of this layer are used as the first 20 nm in a 40 nm thick film, whereas the next 20 nm are fitted with a new layer. Similarly, the 60 nm thick layer is fitted as a superposition of three separate layers. After calculation of the optical interference pattern with these data, the generation of free carriers is calculated by solving a differential equation with the exciton diffusion length (L_D) as a parameter. An exciton blocking boundary condition is used for the ITO-PbPc interface as well as for all PbPc−PbPc interfaces. Moreover, the PbPc layers are assumed to be perfectly flat. This assumption could lead to an overestimation of the exciton diffusion length, as the PbPc layer has a finite roughness which results in an increased donor/acceptor interface area.

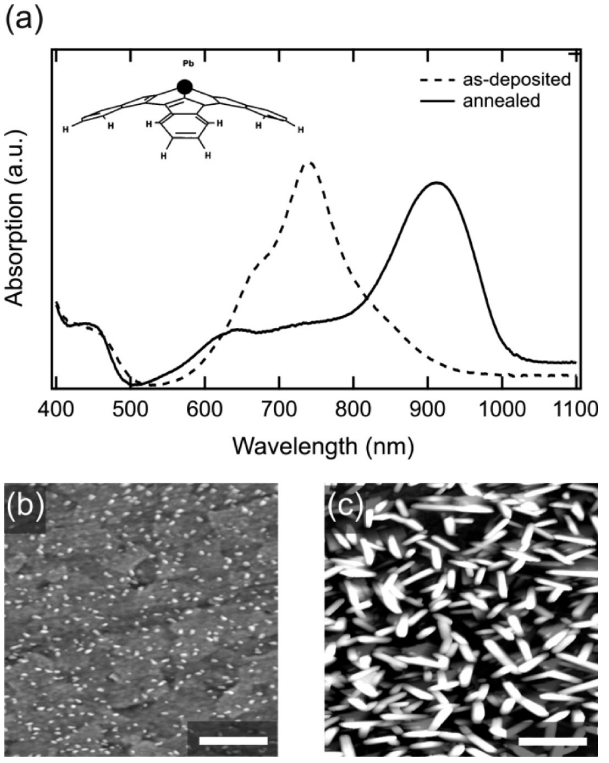

Figure 1. (a) Absorption spectra of a 10 nm PbPc film evaporated at 1 Å/s and 35 °C before (dashed line) and after (solid line) annealing for 2 h at 160 °C in a N_2 atmosphere. The inset shows the chemical structure of the PbPc molecule.[41] Corresponding 2 × 2 μm^2 AFM images of the (b) as-deposited film and (c) annealed film. Values of rms roughness are (b) 6.2 and (c) 26.0 ± 0.5 nm. Horizontal scale bar corresponds to 500 nm.

3. Results

3.1. Thin Film Characterization. First, we examine the effect of deposition conditions on thin film structural evolution by absorption spectroscopy and XRD, whereas film topography is monitored by AFM.

Figure 1a shows the absorption spectra of a 10 nm thick PbPc film deposited at 1 Å/s and 35 °C before and after annealing for 2 h at 160 °C under a nitrogen atmosphere. The absorption of the as-deposited film resembles the solution spectrum, shown in Figure S1 in the Supporting Information for 3×10^{-6} M PbPc in dimethylsulfoxide. The characteristic shape of the Q-band is preserved, albeit with a red-shift of approximately 40 nm and changes in the relative intensities of the vibronic transitions. The annealed film, on the other hand, shows a completely different spectrum, with an intense peak at $\lambda = 900$ nm and two shoulders at $\lambda = 720$ and 655 nm. Images b and c in Figure 1 depict the corresponding AFM images of the as-deposited and annealed film respectively. The 10 nm thick as-deposited film reflects the underlying hexagonal ITO superstructure without displaying the characteristic corrugated ITO structure on nanometer scale. This is indicative for the presence of a continuous wetting layer[33]

(31) Robinson, I. K; Tweet, D. J. *Rep. Prog. Phys.* **1992**, *55*, 599–651.
(32) Pettersson, L. A. A.; Roman, L. S.; Inganäs, O. *J. Appl. Phys.* **1999**, *86*, 487–496.
(33) Gommans, H.; Cheyns, D.; Aernouts, T.; Girotto, C.; Poortmans, J.; Heremans, P. *Adv. Funct. Mater.* **2007**, *17*, 2653–2658.

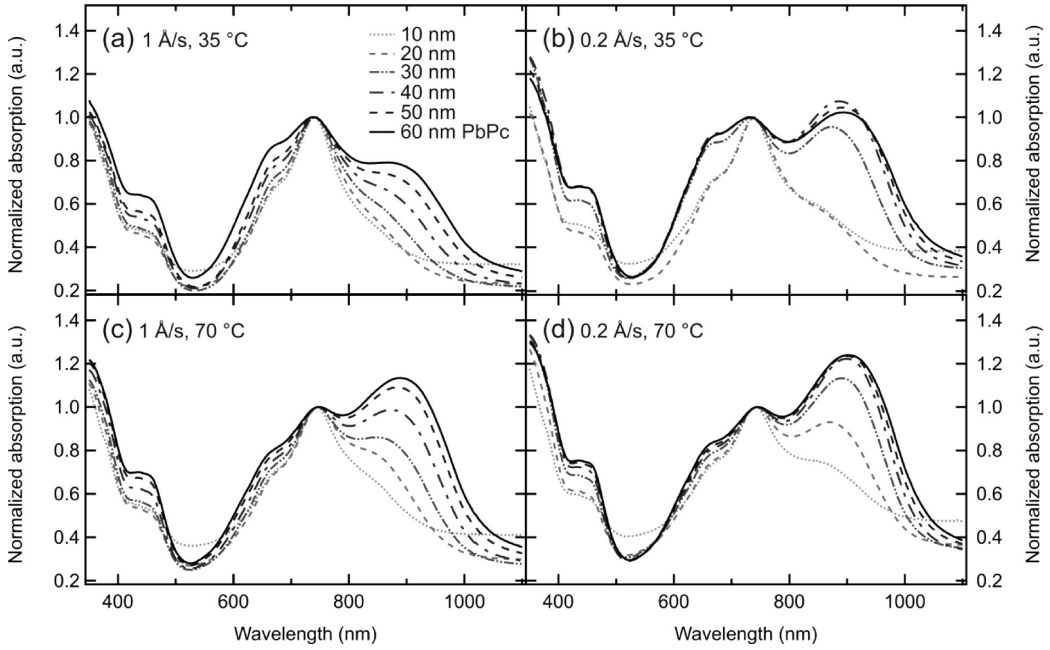

Figure 2. Absorption spectra of PbPc films on glass with thickness varying from 10 to 60 nm, deposited at four different deposition conditions; (a) $r_{dep} = 1$ Å/s and $T_{sub} = 35$ °C, (b) $r_{dep} = 0.2$ Å/s and $T_{sub} = 35$ °C, (c) $r_{dep} = 1$ Å/s and $T_{sub} = 70$ °C, (d) $r_{dep} = 0.2$ Å/s and $T_{sub} = 70$ °C. All spectra are normalized to the absorption peak at $\lambda = 740$ nm.

on top of which crystallites with an approximate diameter of 20 nm have nucleated. Upon annealing, the film morphology changes drastically via the formation of elongated grains, which are approximately 60 nm wide and 300 nm long, causing an increase in root-mean-square (rms) roughness from 6.2 to 26 nm. It should be noted that for all rms roughness values mentioned throughout the text, we have estimated an error margin of ±0.5 nm.

The evolution of the PbPc absorption spectrum with varying film thickness (from 10 to 60 nm) was studied under four different deposition conditions. Figure 2 shows the absorption spectra of films deposited on glass at an evaporation rate of 0.2 and 1 Å/s, both onto a nonheated (T_{sub} = 35 °C) and heated (T_{sub} = 70 °C) substrate. All spectra have been normalized to the peak at $\lambda = 740$ nm, which corresponds to the most intense peak in the absorption spectrum of the monoclinic phase.[24] For all deposition conditions, increasing the film thickness enhances the intensity of the NIR peak with respect to the normalized peak. The rate at which this NIR peak grows with thickness is increased by decreasing the deposition rate (Figure 2b), or by raising the substrate temperature (Figure 2c).

Figure 3 compares the topography of 10 and 60 nm thick films evaporated at 1 Å/s onto a nonheated and heated ITO substrate. At low T_{sub}, both 10 and 60 nm thick films consist of crystallites with a diameter of approximately 20 nm that have nucleated on top of a continuous wetting layer. The main difference between both films is the crystallite density, as the ITO substrate superstructure is still clearly visible for the thinnest film. The latter has an rms roughness value of 6.2 nm, whereas this amounts to 7.5 nm for the 60 nm thick film. Increasing T_{sub} to 70 °C has a marked influence on film topography for an evaporation rate of 1 Å/s (Figure 3c,d); the crystallite density is significantly lower, resulting in a larger grain size[34] and an increased aspect ratio.

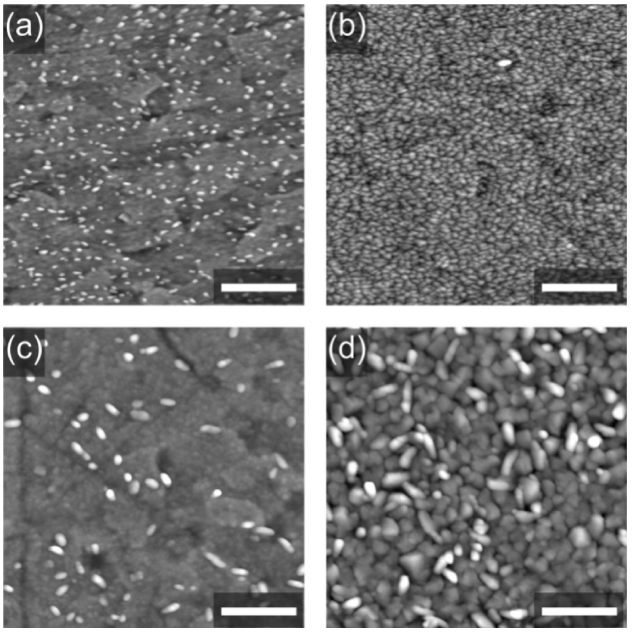

Figure 3. AFM images ($2 \times 2\ \mu m^2$) of films deposited on ITO substrates at $r_{dep} = 1$ Å/s. Films of (a) 10 and (b) 60 nm deposited at $T_{sub} = 35$ °C are compared to films of (c) 10 and (d) 60 nm deposited at $T_{sub} = 70$ °C. Values of rms roughness are (a) 6.2 and (b) 7.0, (c) 5.5 and (d) 11.0 ± 0.5 nm.

Figure 4 shows AFM images of 10 and 60 nm thick films evaporated at 0.2 Å/s onto a nonheated and a heated ITO substrate. At low T_{sub}, the films resemble those deposited at 1 Å/s and 35 °C (cf. Figure 3a and b). The main

(34) Ruiz, R.; Choudhary, D.; Nickel, B.; Toccoli, T.; Chang, K. C.; Mayer, A. C.; Clancy, P.; Blakely, J. M.; Headrick, R. L.; Iannotta, S.; Malliaras, G. G. *Chem. Mater.* **2004**, *16*, 4497–4508.

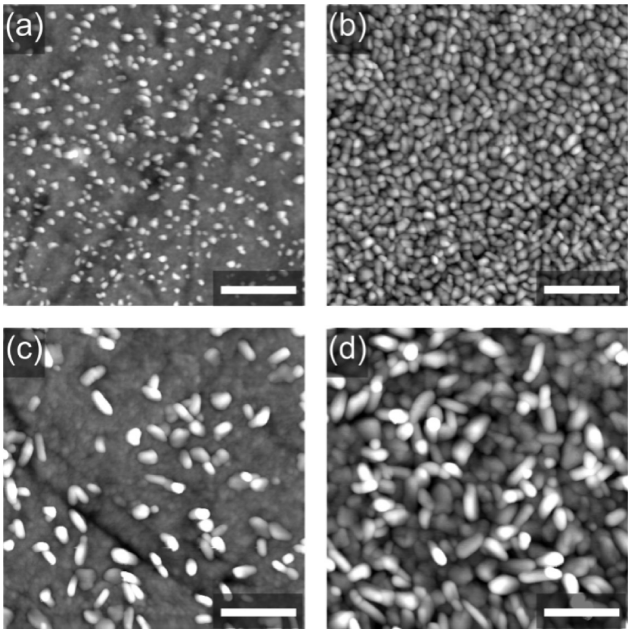

Figure 4. AFM images ($2 \times 2\ \mu m^2$) of films deposited on ITO substrates at $r_{dep} = 0.2$ Å/s. Films of (a) 10 and (b) 60 nm deposited at $T_{sub} = 35$ °C are compared to films of (c) 10 and (d) 60 nm deposited at $T_{sub} = 70$ °C. Values of rms roughness are (a) 8.0 and (b) 10.0, (c) 12.0 and (d) 15.0 ± 0.5 nm.

difference is the increased crystallite size, corresponding to a diameter of approximately 30 nm. This results in an increased rms roughness of 8.0 nm for the thinnest film and 10.0 nm for the thickest film. At elevated substrate temperature, not only crystallite size but also height increased, resulting in rms roughness values of 12.0 and 15.0 nm for the 10 and 60 nm thick films, respectively. In comparison to Figure 3d, the aspect ratio of the grains is increased further.

Another important parameter in film topography is the films microscopic surface area, which takes into account both the pitch and the size of surface features, and therefore provides complementary information to the rms roughness value. The microscopic surface area can be far greater than the geometric area due to surface convolutions[35] and its ratio is a measure for the surface folding. According to this definition, a value of one would correspond to a perfectly flat surface. For the films studied in this work, the calculated folding ratio increases with film thickness and is maximal for 60 nm thick films deposited at 1 Å/s and 35 °C. For this deposition condition, the folding ratio increases from 1.2 to 1.5 ± 0.1 when the layer thickness is increased from 10 to 60 nm. As the crystallite size augments with T_{sub}, the folding ratio drops to 1.2 ± 0.1 for 60 nm thick films deposited at elevated T_{sub} and both low and high r_{dep}.

The performed grazing incidence XRD measurements provides information on the structural evolution and growth of the films, as only the top part of the measured layer contributes to the signal. The measured XRD patterns of PbPc films of 10 and 60 nm thickness, deposited at two different rates and substrate temperatures, as well as after annealing treatment, are shown in Figure 5.

(35) Carolus, D. M.; Bernasek, S. L.; Schwartz, J. *Langmuir* **2005**, *21*, 4236–4239.

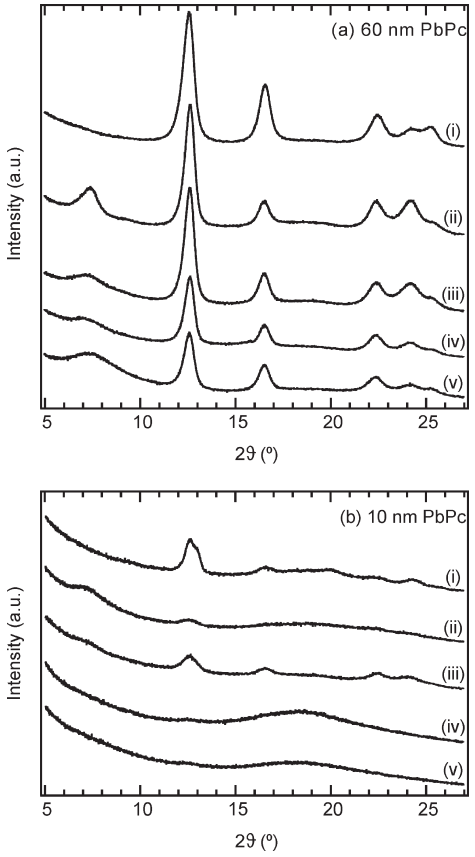

Figure 5. XRD patterns of (a) 60 and (b) 10 nm thick films deposited onto SiO_2 substrates at (i) $r_{dep} = 1$ Å/s and $T_{sub} = 35$ °C, followed by annealing for 2 h at 160 °C in N_2, (ii) $r_{dep} = 0.2$ Å/s and $T_{sub} = 70$ °C, (iii) $r_{dep} = 0.2$ Å/s and $T_{sub} = 35$ °C, (iv) $r_{dep} = 1$ Å/s and $T_{sub} = 70$ °C, (v) $r_{dep} = 1$ Å/s and $T_{sub} = 35$ °C. The vertical dashed lines represent the positions of the calculated diffraction peaks in the triclinic crystal structure, and the dotted lines those in the monoclinic crystal structure. (cf. Table 1).

The XRD patterns of the 60 nm thick films (cf. Figure 5a) are described first, as those have a high signal-to-noise ratio, simplifying the peak deconvolution and analysis. This fitting procedure allows us to investigate the structure of the PbPc films by comparing not only absolute peak intensities, but also relative changes in peak distributions. The peak intensities are highest for the annealed film ((i) in Figure 5a) and decrease for the as-deposited films with increasing r_{dep}, and to a lesser extent with decreasing T_{sub}. Notably, the peak around 7.4° is absent in the XRD pattern of the annealed film.

From the simulated diffraction spectra, we know that M(2 0 0) and T(0 0 1) reflections appear around 6.9°, T(1 $\bar{1}$ 0) and T(1 0 0) around 7.4°, and that the peak at 7.75° corresponds to the M(1 2 0) reflection (cf. Table 1). For the film grown at 1 Å/s and 35 °C ((v) in Figure 5a), this peak is broadened to the right, due to the increased appearance of poorly ordered M(1 2 0) oriented domains. For the film deposited at 0.2 Å/s and 35 °C ((ii) in Figure 5a), this peak is higher and narrower, corresponding to the appearance of relatively more and well-ordered T(1 $\bar{1}$ 0) and T(1 0 0) oriented domains. The average M/T ratio follows the opposite trend as the crystallinity, and increases with increasing r_{dep}, and with decreasing T_{sub}. However, this ratio is smaller than 1 for all films, suggesting that the top structure of the film has a predominantly triclinic structure. The most intense

diffraction peak around 12.5° arises mainly from three different contributions; T(1 1 $\bar{1}$) at 12.12°, T(0 2 0) at 12.35°, and M(3 2 0) at 12.52°. In this case, no clear trend for the evolution of the average M/T ratio with deposition conditions could be discerned. The peak at 16.5° corresponds to triclinic orientations exclusively, and is the highest for the annealed film. Remarkably, this peak is present for all 60 nm thick films, suggesting that all films have triclinic domains. The high-order peaks between 21 and 26° are higher and narrower for the films grown with slower evaporation rates ((ii) and (iii) in Figure 5a), pointing to an improved long-range ordering.

When considering thinner films (cf. Figure 5b), the decreased signal-to-noise ratio points to an overall lower crystallinity compared to the 60 nm thick films. Hence, less conclusive statements can be made on the XRD analysis of the 10 nm thick layers. On the one hand, films deposited at 1 Å/s ((iv) and (v) in Figure 5b) exhibit a broad peak between 16 and 21° and lack distinct diffraction peaks, thereby indicating the monoclinic, albeit poorly crystalline character of these films. On the other hand, deposition at lower rate ((ii) and (iii) in Figure 5b) seems to induce a more triclinic character, as was suggested by resolving the peak around 7.4°. The intensity of the peak around 12.5° is clearly the highest for the annealed film ((i) in Figure 5b), but shows the appearance of another orientation which was not observed for the 60 nm thick annealed film; the T(1 $\bar{2}$ 1) reflection at 13°. Remarkably, the average M/T ratio in the 10 nm thick film is lower than that of the 60 nm thick film.

3.2. Solar Cell Characterization. Next, we evaluate the photoelectrical activity of the studied layers in solar cell structures ITO/PbPc (x)/C_{60} (50 nm)/BCP (10 nm)/Ag, where x denotes the PbPc thickness varying from 10 to 60 nm in steps of 10 nm.

Figure 6 plots J_{SC}, open-circuit voltage (V_{OC}) and PCE of the fabricated solar cells for each growth condition of the donor layer. Solar cells with the PbPc layer deposited at 0.2 Å/s and 70 °C were shunted, likely due to the increased roughness of these films (cf. Figure 4c and d), and are therefore not further considered in this section. For the other three deposition conditions, J_{SC} shows a maximum as a function of PbPc thickness, and this optimum shifts to lower thickness when the donor material is deposited either at lower r_{dep} or at an elevated T_{sub}. The V_{OC} of solar cells based on PbPc deposited at 1 Å/s and 35 °C undulate around 500 mV, whereas this value plunges upon substrate heating, especially for thin donor layers. When r_{dep} is lowered to 0.2 Å/s and T_{sub} is 35 °C, the average V_{OC} value slightly decreases to 470 mV. As the fill factor is 52 ± 3% for all devices, the resulting PCEs follow the trend of J_{SC}. The maximal measured PCE amounted 2.6% with a J_{SC} of 11 mA cm^{-2} for solar cells based on a 40 nm thick PbPc donor layer deposited at 0.2 Å/s and 35 °C.

Figure 7 shows the dark $J-V$ response (a) as well as the $J-V$ curves under illumination (b) for the solar cell based on a PbPc donor layer with a thickness of 40 nm, deposited at different deposition rates and substrate temperatures. It can be seen that the dark current of the device based on a donor layer deposited onto a heated substrate increases, which is accompanied by a decrease in parallel resistance (R_p). The R_p values have been determined by fitting the corresponding dark curves to the classical diode equation [36] and have an average value of $4.4 \times 10^4\ \Omega\ cm^2$ for the solar cells where PbPc is deposited at low T_{sub}, whereas they decrease to $8 \times 10^3\ \Omega\ cm^2$ upon substrate heating. The reverse saturation current (J_0) shows a concomitant rise from 3.6×10^{-8} to 9.1×10^{-7} mA cm^{-2}.

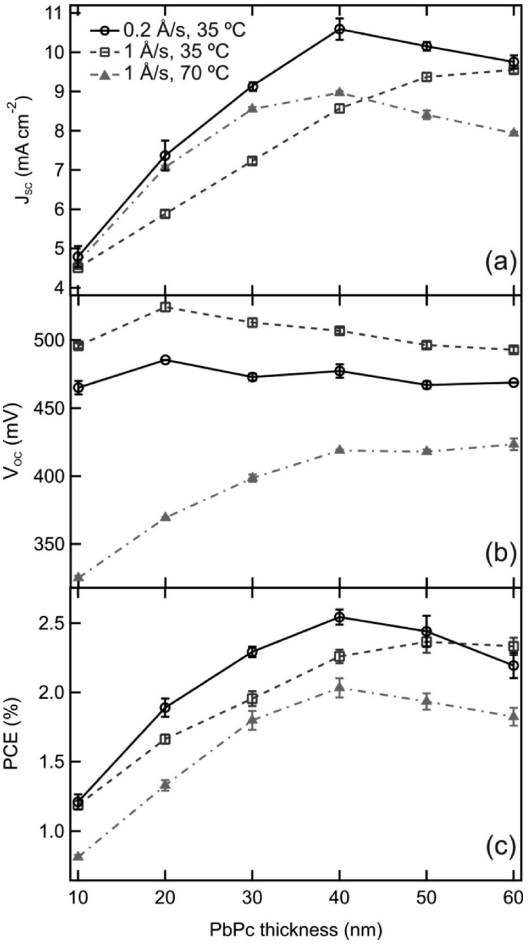

Figure 6. Short-circuit current density (J_{SC}), open-circuit voltage (V_{OC}) and power conversion efficiency (PCE) of solar cells with structure ITO/PbPc (x)/C_{60} (50 nm)/BCP (10 nm)/Ag as a function of PbPc layer thickness (x), and for three different deposition conditions: r_{dep} = 1 Å/s and T_{sub} = 35 °C, r_{dep} = 1 Å/s and T_{sub} = 70 °C, r_{dep} = 0.2 Å/s and T_{sub} = 70 °C.

Figure 8 assembles spectral response data for the devices based on a PbPc donor layer deposited at (a) 1 Å/s and 35 °C, (b) 1 Å/s and 70 °C, and (c) 0.2 Å/s and 35 °C. In these spectra, photocurrent contribution from C_{60} is generated between λ = 350 and 550 nm, and from PbPc between λ = 600 and 1100 nm. For the 10 and 20 nm thick films, all EQE spectra follow the absorption spectra of the constituent layers. At higher donor layer thickness, the peak at λ = 740 nm becomes a dip in the EQE spectrum. In Figure 8a, the NIR contribution from PbPc increases with thickness, and achieves a maximum EQE of 30% at λ = 900 nm. In

(36) Bube, R. H.; Fahrenbruch, A. L. *Advances in Electronics and Electron Physics*; Academic: New York, 1981.

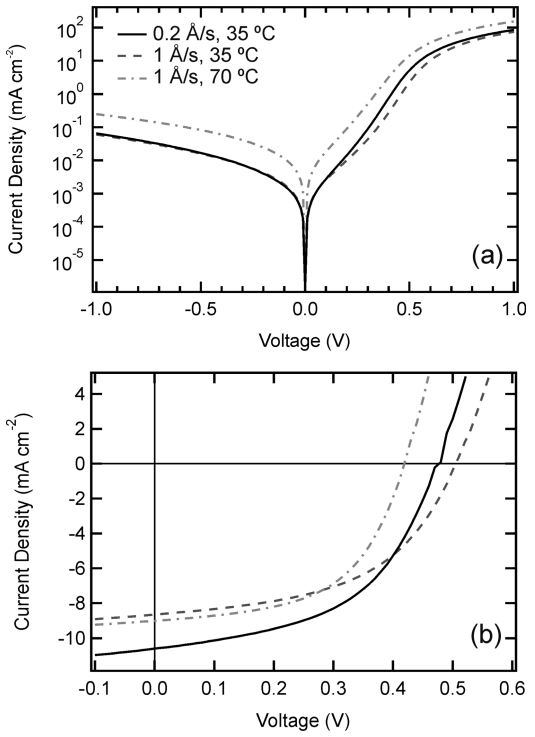

Figure 7. Current density vs voltage characteristics (a) in the dark and (b) under illumination for solar cells with structure ITO/PbPc (40 nm)/C_{60} (50 nm)/BCP (10 nm)/Ag for donor layers deposited at the same conditions as in Figure 6.

Figure 8b, the current generated from the NIR contribution in the absorption spectrum increases rapidly up to a film thickness of 30 nm. Above this thickness, the EQE signal drops to lower efficiency values over the complete wavelength range. For devices based on a donor layer deposited at low rate onto a nonheated substrate (Figure 8c), the same observations as for the spectral response curves shown in Figure 8b are valid up to a donor layer thickness of 30 nm. In this case, the photocurrent response maximizes, exhibiting an EQE peak value of 34% at $\lambda = 900$ nm for the device with a donor layer thickness of 40 nm.

The integration of the EQE data over the standard AM 1.5G spectrum lead for all devices to lower J_{SC}. This difference is caused by multiple intense emission peaks in the Xenon lamp spectrum used by the solar simulator, especially at $\lambda = 820-950$ nm. Consequently, the J_{SC} values of solar cells based on PbPc layers with a dominant absorption peak at $\lambda = 900$ nm are influenced mostly. Calculated J_{SC} values are plotted in Figure 9, and exhibit the same trends as those described for Figure 6. Using the measured *FF* and V_{OC} values, we estimated an AM 1.5G power conversion efficiency which is shown in Figure 9b.

Furthermore, the spectral response data are used for deriving an approximate value for the exciton diffusion length (L_D) by the fitting procedure described in the Experimental Methods. In this model, changes in optical constants with film thickness are accounted for by approximating the mixed PbPc layer as a superposition of multiple uniform layers, with a thickness of 20 nm each (see section 2 for details). Figure 10 shows the fitted optical constants of the subsequent 20 nm thick layers grown

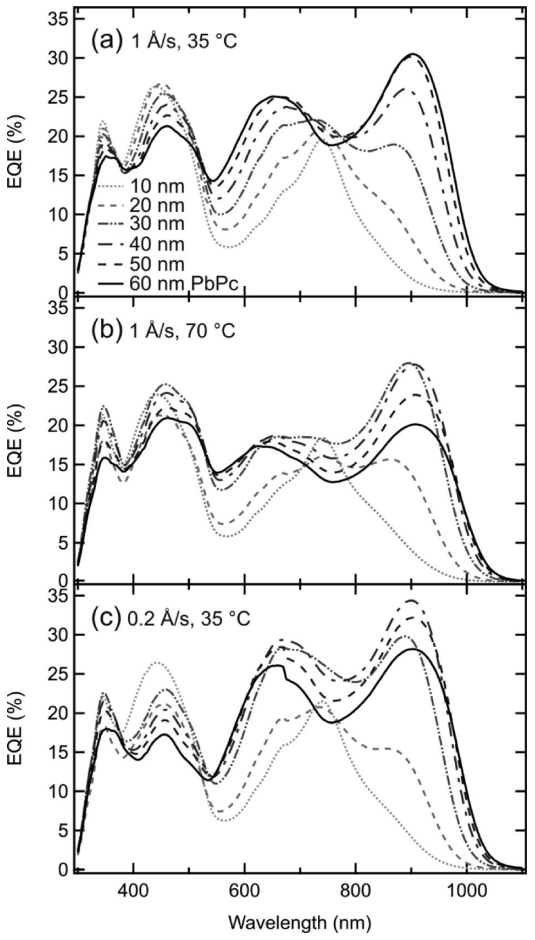

Figure 8. Measured external quantum efficiency (EQE) spectrum for the devices from Figure 6, with the PbPc donor layer deposited at (a) $r_{dep} = 1$ Å/s and $T_{sub} = 35$ °C, (b) $r_{dep} = 1$ Å/s and $T_{sub} = 70$ °C and (c) $r_{dep} = 0.2$ Å/s and $T_{sub} = 70$ °C.

at $r_{dep} = 1$ Å/s and $T_{sub} = 35$ °C. Finally, this procedure allows us to extract an estimated value of $L_D = 5.5$ nm for the 20 nm thick layer, whereas $L_D = 12$ nm is the upper limit for the 40 and 60 nm thick film.

4. Discussion

Lead phthalocyanine is known to have two polymorphs with a marked difference in their absorption spectra. The spectrum of the as-deposited film shown in Figure 1a coincides with that assigned to the monoclinic phase by Collins et al.,[27] whereas the spectrum of the annealed film agrees quite well with that of the triclinic phase.[24] Indeed, it has been shown that a predominantly monoclinic film is formed at moderate deposition rates and low substrate temperatures,[28] and that annealing induces a monoclinic-to-triclinic phase transformation.[25] The presence of mainly triclinic phase for annealed layers is consistent with the XRD patterns, although a monoclinic contribution could still be discerned. Notably, the M/T ratio increases with film thickness, meaning that the top part of the 60 nm thick annealed film has on average more monoclinic structure than the bottom part of the film. This finding might suggest that the annealing time or temperature was too low to induce a phase transition throughout the complete film. Upon comparison

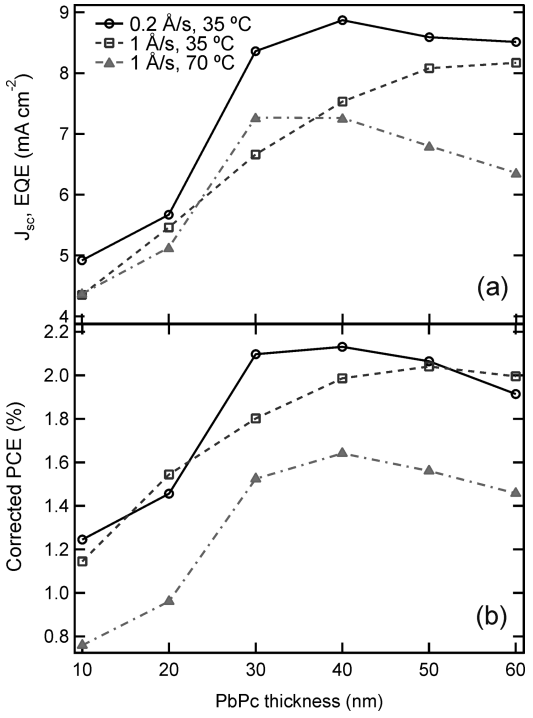

Figure 9. (a) Short-circuit current densities as calculated by integration of the EQE data over the standard AM 1.5G spectrum, and (b) an estimation for the AM 1.5G power conversion efficiencies using the calculated J_{SC} values and the measured V_{OC} (cf. Figure 6b) and *FF*.

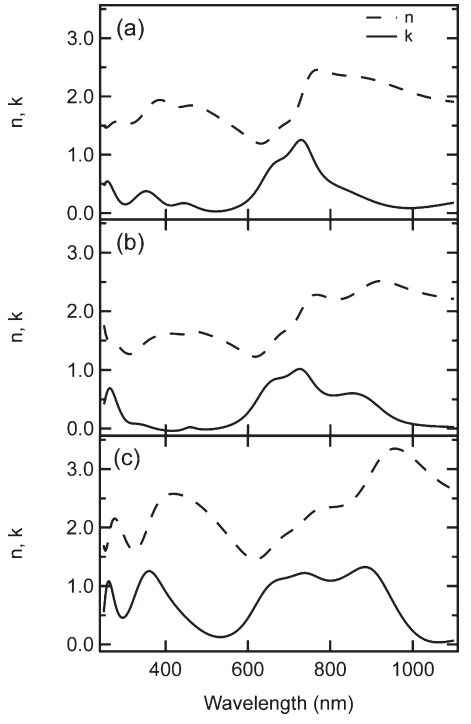

Figure 10. Fitted optical constants of subsequent 20 nm thick layers grown at r_{dep} = 1 Å/s and T_{sub} = 35 °C, employed for modeling a mixed monoclinic−triclinic PbPc layer as a superposition of separate layers: (a) the first layer of 20 nm thickness is fitted using a single layer, and is then (b) superposed to model a layer of 40 nm, and finally is (c) used in combination with the previous two layers to model a 60 nm thick layer.

with the characteristics of the annealed film, both absorption and XRD data suggest that all PbPc films in this study are either of a monoclinic or mixed composition.

First, the evolution of the absorption spectra with thickness shows an increasing NIR absorption peak with respect to the normalizing peak at λ = 740 nm, pointing to an augmenting triclinic contribution in thicker films. The XRD measurements show a large improvement in crystallinity of both monoclinic and triclinic domains when going from 10 to 60 nm thick films. Since we probe preferentially the structure of the top surface with the grazing incidence XRD configuration, this observation indicates the presence of an asymmetric structure in all studied PbPc layers. Close to the substrate surface, the layer is poorly crystalline monoclinic, and evolves to a predominantly triclinic structure in the upper part of the film. As the shift of the absorption spectrum originates from a phase transition from monoclinic to triclinic leading to an increased interaction between the Pc rings,[13,18−20] it is evident that increasing the volume and crystallinity of the triclinic domains promotes the NIR absorption.

Second, the relative intensity of the NIR peak for constant layer thickness was observed to increase by (i) raising the substrate temperature and (ii) decreasing the evaporation rate. The XRD data confirm this trend by showing a concomitant increase in crystallinity of the surface structure of the 60 nm thick layers. As the relative amount of triclinic domains is highest for the film deposited at low r_{dep} and high T_{sub}, the NIR peak in the absorption spectrum shows the most enhancement relative to the normalizing peak at λ = 740 nm. The presence of the T(1 0 0) orientation in this film (cf. (ii) in Figure 5a and 5b) in contrast to the postdeposition annealed film (cf. (i) in Figure 5a and 5b), could indicate that those crystallites are reoriented during the annealing process and either (i) take on an orientation that cannot be detected by this grazing incidence configuration, or (ii) adopt an orientation which is already explicitly present in the film and hence does not have a distinct contribution to the measured XRD pattern. However, absorption characteristics for both films are similar, as these originate from the different packing structure in the triclinic phase, regardless of the apparent crystal orientations.

Finally, we can correlate the structural evolution of the PbPc layers as derived from absorption and XRD data to the performance of heterojunction solar cells with the studied PbPc films as donor layer. For all PbPc layers, the spectral response in the corresponding solar cells reflects the asymmetric layer structure originating from the increasing triclinic character with thickness. From a donor layer thickness of approximately 30 nm onward, the peak at λ = 740 nm corresponding to the dominant peak in the monoclinic absorption spectrum, becomes a dip. In other words, since only excitons generated nearby the PbPc/C_{60} interface can effectively contribute to photocurrent, the poorly ordered monoclinic portion of the film near the ITO substrate filters this light from being absorbed in the portion of the film within one exciton diffusion length (L_D) away from the donor/acceptor interface.

For the film deposited at 1 Å/s onto a nonheated substrate, the EQE spectra follow the increasing NIR absorption of the PbPc layer with increasing thickness.

This indicates that the upper part of the layer, which mainly consists of triclinic domains, entirely contributes to the photocurrent. In order to verify the increase in photogenerated J_{SC} with film thickness, an approximate value for L_D is derived from fitting the spectral response data as described in the Experimental Methods. As this model assumes perfectly flat PbPc layers, it should be verified that the increased donor/acceptor area is not causing an apparent increase in L_D. When comparing the folding ratio of a 10 nm thick film deposited at 1 Å/s and T_{sub} = 35 °C to the 60 nm thick film grown at the same conditions, an increase of 25% is observed. However, this increment is insufficient to explain a 2-fold increase in L_D. As thicker films exhibit both an increased triclinic character as well as an enhanced crystallinity, it is difficult to determine which effect has the dominant impact to the substantial increase in L_D.[37]

For solar cells based on PbPc layers deposited at high T_{sub} or low r_{dep}, J_{SC} starts to drop at lower donor layer thickness due to the promotion of the triclinic structure under these conditions. As can be seen from Figure 10, a layer with increased triclinic content and improved crystallinity exhibits a higher extinction coefficient and broader absorption. The highest EQE peak value of 34% at λ = 900 nm was obtained for the device based on the 40 nm thick donor layer deposited at low r_{dep}. Compared to a solar cell with a donor layer deposited at high T_{sub}, on the one hand, the maximal J_{SC} value is 26% higher. (cf. Figure 10a) However, the folding ratio of the layer grown at low r_{dep} is 17% higher than that of the layer deposited at high T_{sub}. In this case, the increase in diffusion length can be correlated with an increase in donor/acceptor interface area. Compared to a solar cell with the donor layers deposited at 1 Å/s and low T_{sub}, on the other hand, the maximal photocurrent value is 9% higher, and the folding ratio is lower for the film grown at low r_{dep}. This means that an increased L_D is observed for films deposited at low r_{dep} and high T_{sub}, which can be attributed to the increased triclinic character and/or the enhanced crystallinity of those films.

Ideally, J_{SC} should be maximized by extending the absorption of the donor layer toward the NIR, without reducing the V_{OC}, because this would optimize the overall performance of the solar cell. In order to optimize J_{SC}, a predominantly triclinic film is desirable. Unfortunately, as the HOMO level of PbPc becomes shallower for layers that have been heat treated or were deposited at low r_{dep}[38] and since V_{OC} of the solar cell is known to be determined by the energetics of the donor−acceptor interface,[39,40] triclinic donor layers will lead to solar cells with lower V_{OC} compared with devices employing monoclinic layers. This corresponds to our observations, since devices based on donor layers exhibiting a predominantly monoclinic character yielded the highest V_{OC} values. However, not only band-edge energies play a role in V_{OC}. The increased roughness of the layers induced by high-temperature deposition leads to a reduction in V_{OC} due to an increased J_0 and decreased R_p value.[40] In the most extreme case, when a low deposition rate was combined with a high substrate temperature, the high roughness of the resulting layer (cf. Figure 4d) indicates a higher possibility of including voids in the PbPc layer, which then creates shunt paths for C_{60}. This is the most likely cause for shorting of all devices fabricated under the above-mentioned conditions.

The layers that exhibit both an improved crystallinity and triclinic content due to the lower r_{dep}, lead to solar cells with a V_{OC} that is only slightly smaller than that of the solar cell based on the primarily monoclinic film. Consequently, such layers yield the best performing solar cells, as fill factors remain constant for all devices. Because of the higher exciton diffusion length in this predominantly triclinic layer, the photocurrent increased to 11 mA cm^{-2} for a solar cell based on a 40 nm thick PbPc film. With a V_{OC} of 477 mV and a fill factor of 52%, this solar cell yields a maximal PCE of 2.6%. Moreover, with a broad EQE signal above 11% from λ = 320−990 nm, this is a well-performing NIR-sensitive solar cell.

5. Conclusion

We investigated the structural evolution of PbPc layers grown under various deposition conditions by both absorption spectroscopy and XRD measurements. Mixed monoclinic (M)−triclinic (T) layers with an enhanced NIR absorption have been obtained by (i) increasing the thickness, (ii) raising the substrate temperature, and (iii) decreasing the evaporation rate. It was shown that these PbPc films exhibit an asymmetric layer structure with a poorly crystalline monoclinic film close to the substrate, evolving to a predominantly triclinic structure in the upper part of the film. Moreover, the enhancement of the NIR peak in the absorption spectrum is mainly correlated to the increased appearance and crystallinity of the triclinic domains in the donor layer. The 60 nm thick films deposited at a relatively low rate of 0.2 Å/s and elevated substrate temperature of 70 °C exhibit the lowest M/T ratio and an enhanced crystallinity, and consequently the highest NIR absorption peak.

Insights in structural evolution of evaporated PbPc films by varying deposition conditions are gained and can be applied to produce layers with a predominantly triclinic structure, inducing an absorption spectrum extended to the NIR, particularly relevant for the fabrication of solar cells with increased spectral coverage. Measured J_{SC} values show a maximum as a function of PbPc layer thickness that is sensitively dependent on the deposition conditions, and hence on the structural evolution in this layer. Layers in which the amount and crystallinity of triclinic domains is increased by lowering r_{dep} or increasing

(37) Lunt, R. R.; Benziger, J. B.; Forrest, S. R. *Adv. Mater.* **2010**, *22*, 1233–1236.
(38) Ikushima, A. J.; Kanno, T.; Yoshida, S.; Maeda, A. *Thin Solid Films* **1996**, *273*, 35–38.
(39) Cheyns, D.; Poortmans, J.; Heremans, P.; Deibel, C.; Verlaak, S.; Rand, B. P.; Genoe *J. Phys. Rev. B* **2008**, *77*, 165332.
(40) Rand, B. P.; Burk, D. P.; Forrest, S. R. *Phys. Rev. B* **2007**, *75*, 115327.
(41) Papageorgiou, N.; Ferro, Y.; Salomon, E.; Allouche, A.; Layet, J. M.; Giovanelli, L.; Le Lay, G. *Phys. Rev. B* **2003**, *68*, 235105.

T_{sub} exhibit a substantial increase in exciton diffusion length when compared to semicrystalline monoclinic layers, as suggested by fitting the spectral response data. In particular, lowering r_{dep} yields in solar cells with a maximal J_{SC} of more than 10% higher than optimized devices consisting of a PbPc layer with a higher relative amount of monoclinic domains. The corresponding EQE is higher than 11% from $\lambda = 320-990$ nm with a peak value of over 34% at $\lambda = 900$ nm, thereby showing the relevance of structural control of the PbPc donor layer in order to achieve high-performance NIR-sensitive solar cells.

Acknowledgment. The authors thank Kristiaan Temst for fruitful discussions and Dimitri Soccol for help with the XRD analysis. The research leading to these results has received funding from the European Community's Seventh Framework Programme (FP7/2007-2013) under grant agreement 212311 of the ONE-P project. K.V. acknowledges the Institute for the Promotion of Innovation through Science and Technology in Flanders (IWT-Vlaanderen) for financial support.

Supporting Information Available: The solution absorption spectrum of approximately 3×10^{-6} M PbPc in dimethylsulfoxide is shown in Figure S1 (PDF). This material is available free of charge via the Internet at http://pubs.acs.org.

Note Added after ASAP Publication. The captions for Figures 9 and 10 were switched in the version published ASAP November 17, 2010; the corrected version was published ASAP November 19, 2010.